Journal of Sound and Vibration (1997) **207**(2), 137–149

GLOBAL BEHAVIOR OF A BIASED NON-LINEAR OSCILLATOR UNDER EXTERNAL AND PARAMETRIC EXCITATIONS

N. E. SANCHEZ

Department of Mechanical Engineering, *University of Texas at San Antonio*, *San Antonio*, *Texas* 78249, *U.S.A.*

AND

A. H. NAYFEH

Department of Engineering Science and Mechanics, *Virginia Polytechnic Institute and State University*, *Blacksburg*, *Virginia* 24061, *U.S.A.*

(*Received* 31 *October* 1995, *and in final form* 19 *February* 1997)

In this work we expand our research on the global behavior of non-linear oscillators under external and parametric excitations. We consider a non-linear oscillator simultaneously excited by parametric and external functions. The oscillator has a bias parameter that breaks the symmetry of the motion. The example that we use to illustrate the problem is the rolling oscillation of a biased ship in longitudinal waves, but many mechanical systems display similar features. The global behavior of the system is characterized by bifurcation diagrams that identify the instabilities that appear when one of the excitations is slowly varied. The locus of these instabilities provides the stability boundaries of the system in a parameter space of physical significance. We found that the dynamics of the system significantly depends on the bias parameter, which confirms previous experimental observations. We also found a very interesting effect, which appears to result from the interaction between the parametric and external responses in a nonlinear manner and causes the primary response to lose stability. All results were obtained through analog simulation of the governing equation.

1. INTRODUCTION

The governing equation of a one-degree-of-freedom (one-DOF) oscillator typically shows excitations that appear as either an inhomogeneity in the differential equation or a time-varying coefficient. These types of excitations are usually called external and parametric excitations, respectively. A number of important problems commonly include both types of excitations. Examples include the vibration of slightly curved rods under a periodic axial force [1] and the roll motion of a biased ship in longitudinal waves [2]. In this work, we expand previous research on non-linear oscillators being excited either externally [3] or parametrically [4]. On this occasion, we consider a non-linear oscillator simultaneously excited by parametric and external functions. Furthermore, this oscillator has a bias parameter that breaks the symmetry of the motion. Our aim is to gain a qualitative understanding of the dynamics by identifying the instabilities that appear when one of the excitations is slowly varied. Even on an analog computer, unstable solutions can appear and with time disappear, or merge with another solution. At the same time, we characterize the loci of these instabilities as the stability boundaries of the system in

0022–460X/97/420137 + 13 $25.00/0/sv970995

a parameter space of physical significance that can occur in reality. In this case, the analysis is carried out for a parameter space that includes broad portions of the amplitude and frequency of the external excitation, at a fixed level of the parametric excitation for the case of a model boat previously used [5]. The simulation of the differential equation is carried out in an analog computer which has, in the past, given good accuracy for the external [3] and the parametric excitations [4]. In recent publications, Liaw and Bishop [6] have investigated the non-linear coupling of heave–roll and ships rolling analytically and numerically, and Perez and Sanguinetti [7] have investigated experimentally the roll in longitudinal waves. They both found the danger of transitions from small oscillations to large oscillations by changing a parameter such as frequency. They also found complicated behavior, but most of the results correlated well with the analytical solutions.

2. GOVERNING EQUATION

We can follow either Wright and Marshfield [5] or Bolotin [1], to derive the equation of motion for either the rolling motion of a ship or the bending of a rod. We present here the results for the case of the ship, since this governing equation is more general, and its application is of fundamental importance for safety and design considerations. Furthermore, the specific mechanisms that cause a vessel to capsize are still not fully understood [8, 9], so we hope that this analysis can shed some light on this fundamental problem.

As shown in Figure 1, the rolling motion of a biased ship can be described by the absolute roll angle $\phi(t)$ and the relative roll angle $\theta(t)$ with respect to the local wave slope $\alpha(t)$. Applying Newton's second law, we find that the equation of motion can be written as

$$(I + \delta I)\ddot{\theta} + D(\dot{\theta}) + K(\theta, \tau, \gamma) = B - I\ddot{\alpha}, \qquad \theta = \phi - \alpha,$$

where I is the roll moment of inertia, δI is the added moment of inertia due to the fluid, which is assumed to be constant [5], and B is a constant bias moment, which might be due to steady wind, or a shift in cargo, or water or ice on deck. The righting arm (restoring moment) $K(\theta, \tau, \gamma)$ this time depends on the angle in which the wave hits the ship and the relative velocity of the wave with respect to the ship. We follow Blocki [10] and obtain the following relation for the rolling of a ship due to heave–roll coupling

$$K(\theta, \tau, \gamma) = \omega^2[\theta + \alpha_3\theta^3\alpha_5 + \theta^5 + h\theta \cos(\tilde{\Omega}\tau + \gamma)],$$

where τ is time and

$$h = K_{\theta z}a_z/2\omega_0^2$$

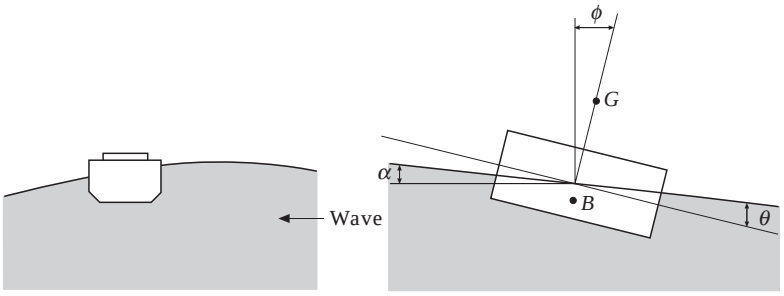

Figure 1. A ship rolling in longitudinal waves with local wave slope α. The ship is biased at an angle ϕ, so that the relative angle with respect to the wave is $\theta = \phi - \alpha$.

represents the magnitude of the parametric excitation, which depends on the coupling cofficient K_{0z} and the amplitude of the heaving motion a_z. A simple one-DOF system is used to describe the basic features of the motion [11]. If we consider the case of waves approaching the ship from the side at an angle γ, the one-DOF resulting motion can be described by

$$\ddot{\theta} + 2\tilde{\mu}\dot{\theta} + \tilde{\mu}_3\dot{\theta}^3 + \omega_0^2[\theta + \alpha_3\theta^3 + \alpha_5\theta^5 + h\theta\cos(\tilde{\Omega}\tau + \gamma)$$

$$= \omega_0^2[\theta_s + \alpha_3\theta_s^3 + \alpha_5\theta_s^5] + \frac{\alpha_m I}{(I + \delta I)}(\tilde{\Omega})^2\cos(\tilde{\Omega}\tau + \gamma). \quad (1)$$

The ship is biased in the sense that it is subjected to a constant heeling moment that tilts the vessel by an angle θ_s. The wavelength is assumed to be large compared with the ship's width. The waves are also assumed to be sinusoidal with a maximum wave slope α_m. Typical waves in the Atlantic Ocean have lengths ranging from 50 to 100 m and heights that are independent of the wavelength [12]. The symbol I represents the roll moment of inertia and δI is the added moment of inertia due to the fluid. The angle γ represents a phase difference between the wave and the heave motion of the ship. The parameter h represents the amplitude of the parametric excitation. It depends on the magnitude of the coupling coefficient and the amplitude of the heaving motion [11, 12]. Equation (1) can be simplified by scaling time according to $t = \omega_0\tau$, resulting in

$$\ddot{\theta} + 2\mu\dot{\theta} + \mu_3\dot{\theta}^3 + \theta + \alpha_3\theta^3 + \alpha_5\theta^5 + h\theta\cos(\Omega t) = \theta_s + \alpha_3\theta_s^3 + \alpha_5\theta_s^5 + F\cos(\Omega t), \quad (2)$$

$$F = \alpha_m I\Omega^2/(I + \delta I),$$

where θ_s is the bias angle and represents the external excitation characterized by the maximum wave slope α_m, the wave frequency Ω, the ship's inertia I and the fluid's added inertia δI. The inertia factor is computed with the relation $I = mK^2$. Using the transformation equation $\theta = \theta_s + u$, we write equation (2) as

$$\ddot{u} + 2\mu\dot{u} + \mu_3\dot{u}^3 + u + b_1u + b_2u^2 + b_3u^3 + b_4u^4 + b_5u^5 + hu\cos(\Omega t) = f\cos(\Omega t), \quad (3)$$

where $b_1 = 3\alpha_3\theta_s^2 + 5\alpha_5\theta_s^4$, $b_2 = 3\alpha_3\theta_s + 10\alpha_5\theta_s^3$, $b_3 = \alpha_3 + 10\alpha_5\theta_s^2$, $b_4 = 5\alpha_5\theta_s$, $b_5 = \alpha_5$ and $f = F - h\theta_s$. Equation (3) is general and can model a wide variety of oscillators. Our interest is to study the effect of the external and parametric excitations on systems that can be symmetric or biased. The parameters α_m, h and Ω are used to characterize the response and stability of the system. One of the features of this systems is that equation (3) lacks symmetry when θ_s is not zero. For example, Wright and Marshfield [5] observed experimentally that the dynamic response and stability of ship models with positive and negative bias angles are different. We characterized ship oscillations for bias angles of $\theta_s = \pm 6^\circ$ and our results fully support the above observation.

3. STABILITY AND BIFURCATION OF SOLUTIONS

Equation (3) is a non-linear ordinary differential equation. To determine the global behavior of the system described by this equation, we observe the solutions shown by the analog computer for different values of the parameters. These solutions can be transient, and disappear given some time of simulation. In order to be sure that a particular solution is not a transient, we use different methods of observing the solution. Verhulst [13] has given definitions to characterize the stability and asymptotic stability of a periodic solution. A periodic solution can be visualized as an orbit in phase space. In this case, a two-dimensional space V can be defined transversal to the closed orbit. The orbit intersects

V at point η, which implies that η is mapped into V by the phase flow. This map is the Poincaré map P and η is a fixed point of P. In this case, we can state the following.

3.1. DEFINITIONS

For the system described by equation (3) with a periodic solution $\phi(t)$, transversal set V and Poincaré map P with fixed point η, the solution $\phi(t)$ is stable if, for each $\varepsilon > 0$, we can find a $\delta(\varepsilon)$ such that

$$\| x_0 - \eta \| \leqslant \delta, \quad x_0 \in V \Rightarrow \| P^n(x_0) - \| \leqslant \epsilon, \qquad n = 1, 2, 3, \ldots .$$

The solution $\phi(t)$ is asymptotically stable if it is stable and if there exists a $\delta > 0$ such that

$$\| x_0 - \eta \| \leqslant \delta, \qquad x_0 \in V \Rightarrow \lim_{n \to \infty} P^n(x_0) = \eta.$$

The above definitions can be implemented by using the so-called Floquet theory [14] numerically to determine if a particular orbit is stable. In the current case, if the solution is stable the analog computer will show it. If it is not stable, there would be a jump to another solution or to an overflow, given enough time.

The best understanding of the behavior of the system can be obtained when the key coefficients of the differential equation are used as parameters and the qualitative effects of slow changes in these parameters are understood. The locations in the parameter space at which the response has qualitative changes are defined as bifurcation points. At these locations the behavior of the system changes, and the new behavior might bring about catastrophic consequences.

In this paper, stable solutions of equation (3) were searched for by using α_m and Ω as parameters. An analog computer system was used to simulate equation (3), and the response observed was processed by using fast Fourier transforms (FFT) and Poincaré maps to identify the bifurcation points.

4. DYNAMICS OF UNBIASED SYSTEM

The response of the system described by equation (3) for the unbiased case is presented first for $\theta_s = 0$, $\gamma = 0$, $h = 0{\cdot}3$ and the other coefficients as given in Table 1. The simulation results are summarized in the bifurcation diagram shown in Figure 2, where the loci of the instabilities are shown. When a parameter (Ω or α_m) is varied across a boundary in the direction marked by the arrow, the current solution will become unstable and the system response will move to a new solution. The bifurcation diagram shows the behavior of three basic attractors (solutions in phase space), which are stable near $\Omega = 1$ and $\Omega = 2$. In Figure 3 is shown a phase diagram of the two stable attractors at $\Omega = 0{\cdot}856$ and $\alpha_m = 0{\cdot}048$. These attractors are T-periodic; that is, they correspond to the primary response of the system. The small attractor loses stability when the parameters are varied across the boundary marked S_1 in Figure 2, which is the locus of saddle-node bifurcations [15] that make the system jump to another attractor. If the crossing occurs for values of $\alpha_m > l_2$, the solution becomes unbounded (the

TABLE 1

System parameters

ω_0	μ	μ_3	α_3	α_5	δI
5·278	0·086	0·108	−1·402	0·271	0·25I

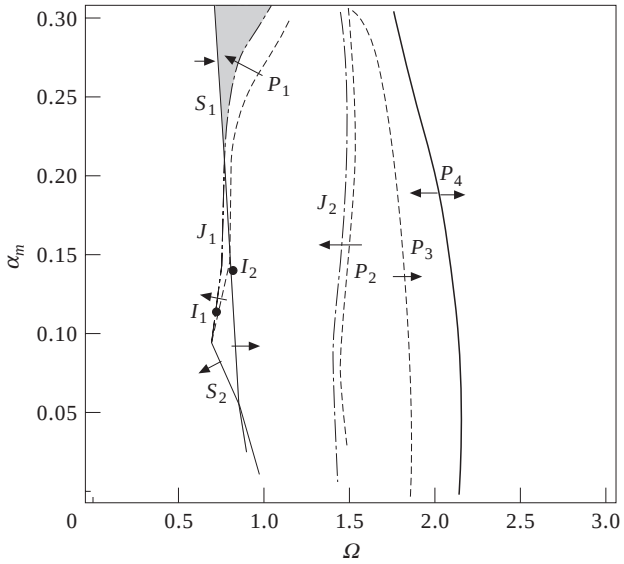

Figure 2. A bifurcation diagram from analog computer simulations of equation (3) for $\gamma = 0$, $\theta_s = 0^\circ$ and $h = 0{\cdot}3$.

ship capsizes). For crossings with values of $\alpha_m < l_2$, the jump is to the large attractor in Figure 3. Similarly S_2 is the locus of saddle-node bifurcations that produce a jump from the large to the small attractor. The large attractor also undergoes a period-doubling sequence to chaos [15] in the region between P_1 and J_1. In Figure 4 are shown phase diagrams and power spectra of various attractors at selected locations in this region. To the right of each phase diagram, two power spectra are shown. The bottom one shows the frequency content of the excitation, and the top one shows the frequency content of the response. In the dotted region of Figure 2, all initial conditions lead to unbounded solutions. When J_1 is crossed, the chaotic attractor loses stability and the system jumps either to an unbounded solution or to the small attractor, depending on whether the crossing occurs above or below l_1.

The large attractor in Figure 3 also loses stability near $\Omega = 2$. Between P_3 and P_4, this attractor is unstable. When P_3 is crossed from left to right, the attractor undergoes a

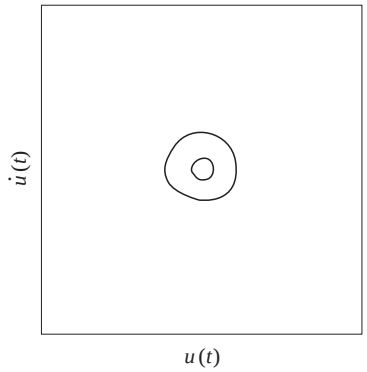

Figure 3. The phase portrait of coexisting attractors at $\Omega = 0{\cdot}856$ and $\alpha_m = 0{\cdot}048$. Both attractors correspond to the primary resonance.

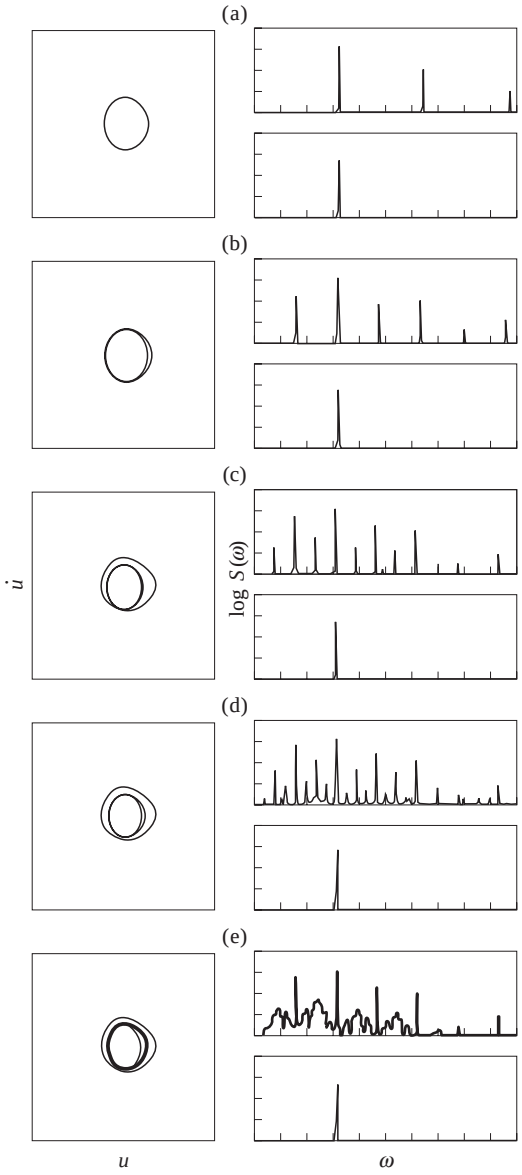

Figure 4. Phase portraits and power spectra of the attractor and the excitation at selected locations near the primary resonance: (a) the T-periodic solution for $\Omega = 0{\cdot}983$ and $\alpha_m = 0{\cdot}258$; (b) the 2T-periodic solution for $\Omega = 0{\cdot}966$ and $\alpha_m = 0{\cdot}268$; (c) the 4T-periodic solution for $\Omega = 0{\cdot}942$ and $\alpha_m = 0{\cdot}282$; (d) the 8T-periodic solution for $\Omega = 0{\cdot}939$ and $\alpha_m = 0{\cdot}284$; (e) the chaotic attractor for $\Omega = 0{\cdot}937$ and $\alpha_m = 0{\cdot}285$.

period-doubling bifurcation and a jump to the subharmonic resonance is observed. When P_4 is crossed from right to left, another period-doubling bifurcation is observed with a jump to the subharmonic response. Therefore, the primary resonance is unstable in the region between P_3 and P_4. The third attractor represented in the bifurcation diagram in Figure 2 is the subharmonic (or 2T-periodic) response near $\Omega = 2$, which is stable in the region between P_4 and J_2. Selected attractors and their power spectra in this region

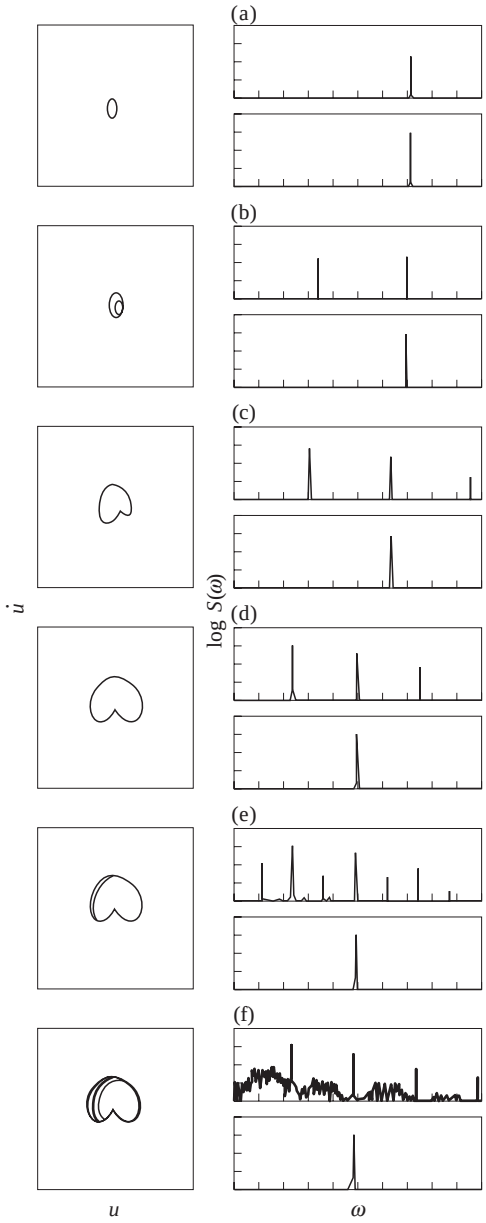

Figure 5. Phase portraits and power spectra of the attractor and the excitation at selected locations near the subharmonic resonance: (a) the primary response for $\Omega = 2{\cdot}158$ and $\alpha_m = 0{\cdot}107$; (b) the subharmonic response for $\Omega = 2{\cdot}102$ and $\alpha_m = 0{\cdot}113$; (c) the subharmonic response $\Omega = 1{\cdot}920$ and $\alpha_m = 0{\cdot}136$; (d) the subharmonic response for $\Omega = 1{\cdot}514$ and $\alpha_m = 0{\cdot}218$; (e) the 2T-periodic subharmonic response for $\Omega = 1{\cdot}505$ and $\alpha_m = 0{\cdot}221$; (f) the chaotic attractor in the subharmonic response for $\Omega = 1{\cdot}480$ and $\alpha_m = 0{\cdot}228$.

are shown in Figure 5: (a) shows the principal-resonance response (top), (b) shows the subharmonic resonance obtained after crossing P_4 from right to left, (c) and (d) show quantitative changes in the subharmonic response, (e) shows the subharmonic response after a period-doubling bifurcation across P_2, and (f) shows a chaotic attractor to the right of J_2.

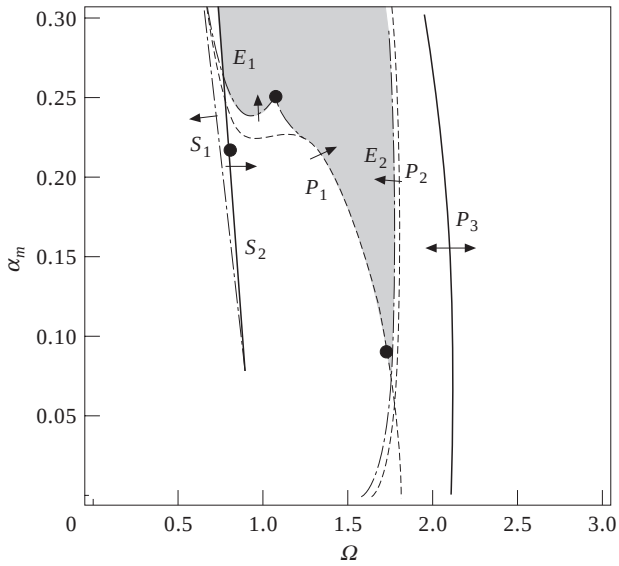

Figure 6. The bifurcation diagram from analog computer simulations of equation (3) for $\gamma = 0$, $\theta_s = +6^\circ$ and $h = 0{\cdot}3$.

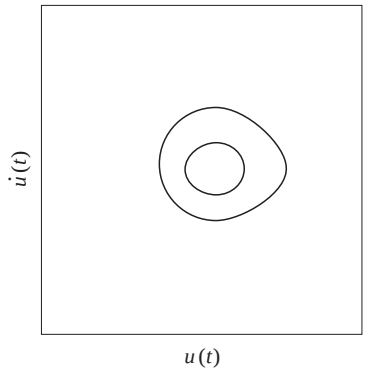

Figure 7. The coexisting attractors near the primary resonance for $\Omega = 0{\cdot}768$ and $\alpha_m = 0{\cdot}217$.

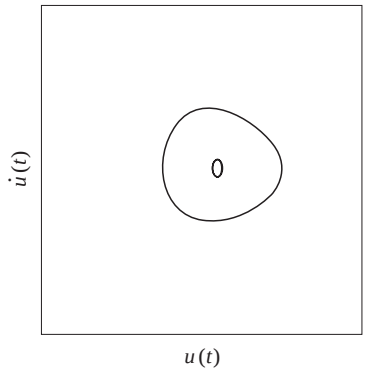

Figure 8. The coexisting attractors near the subharmonic resonance for $\Omega = 1{\cdot}758$ and $\alpha = 0{\cdot}046$.

5. DYNAMICS OF BIASED SYSTEM

In Figure 6 is shown the bifurcation diagram obtained from an analog computer simulation of equation (3) when the bias angle θ_s is set to $+6^\circ$ and all other parameters are left unchanged. In this case the dotted region is many times larger than that for the unbiased system. The region of stability of the subharmonic response has shrunk, and the primary and subharmonic responses only coexist in a narrow region between $\Omega = 1{\cdot}5$ and $\Omega = 2{\cdot}0$.

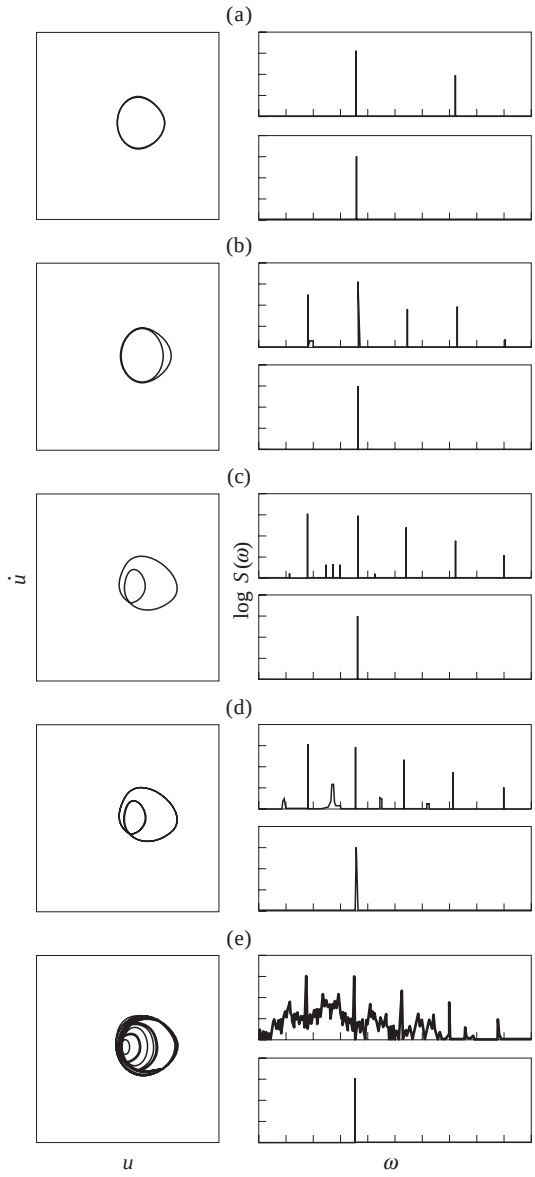

Figure 9. Phase portraits and power spectra of the response and the excitation near the primary resonance: (a) the T-periodic response for $\Omega = 1{\cdot}098$ and $\alpha_m = 0{\cdot}228$; (b) the 2-T-periodic response for $\Omega = 1{\cdot}098$ and $\alpha_m = 0{\cdot}231$; (c) the 2T-periodic response for $\Omega = 1{\cdot}098$ and $\alpha_m = 0{\cdot}245$; (d) the appearance of broadband frequency content in the 2T-periodic response for $\Omega = 1{\cdot}098$ and $\alpha_m = 0{\cdot}248$; (e) the chaotic attractor for $\Omega = 1{\cdot}067$ and $\alpha_m = 0{\cdot}249$.

The curves S_1 and S_2 represent saddle-node bifurcations of the large and small attractors of the primary resonance, which produce jumps in the corresponding attractors. In Figure 7 are shown the two stable attractors for $\Omega = 0{\cdot}768$ and $\alpha_m = 0{\cdot}217$. In Figure 6, S_1 represents the locus of jumps from the large to the small attractor. Similarly, S_2 represents the locus jumps in the small attractor, which take the system either to the large attractor if α_m is below the black dot or to an unbounded solution if it is above this point. The curve P_1 represents the locus of period-doubling bifurcations, which lead the system

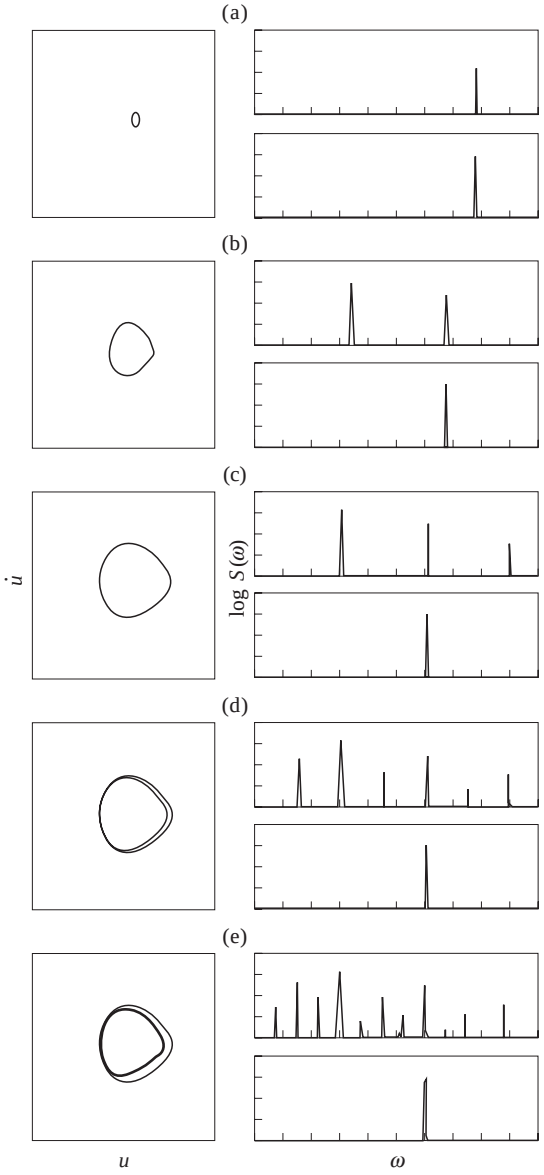

Figure 10. Phase portraits and power spectra of the response and the excitation near the subharmonic resonance: (a) the primary response for $\Omega = 2{\cdot}319$ and $\alpha_m = 0{\cdot}058$; (b) the subharmonic response for $\Omega = 1{\cdot}997$ and $\alpha_m = 0{\cdot}078$; (c) the subharmonic response for $\Omega = 1{\cdot}794$ and $\alpha_m = 0{\cdot}097$; (d) the 2T-periodic attractor of the subharmonic response for $\Omega = 1{\cdot}780$ and $\alpha_m = 0{\cdot}099$; (e) the 4T-periodic attractor of the subharmonic response for $\Omega = 1{\cdot}763$ and $\alpha_m = 0{\cdot}100$.

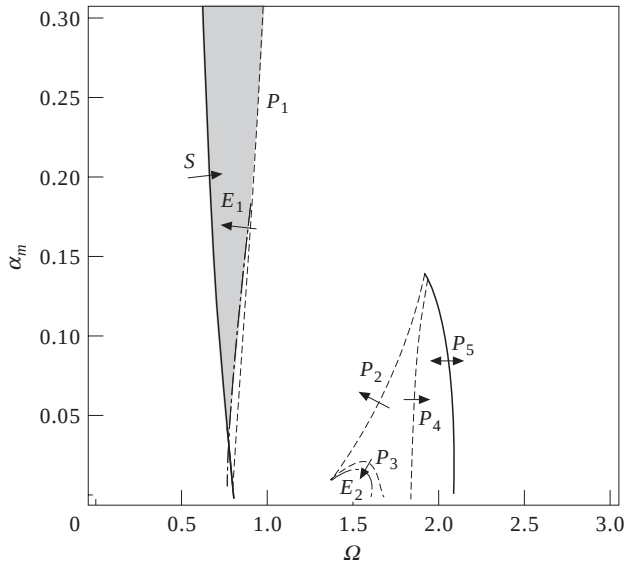

Figure 11. The bifurcation diagram from analog computer simulations of equation (3) for $\gamma = 0$, $\theta_s = -6^\circ$ and $h = 0{\cdot}3$.

to either a period-doubling sequence to chaos in the portion of the curve enclosed by E_1 or directly to an instability in the rest of the curve. The instability results in an unbounded solution when α_m is above the black dot on the lower part of P_1, or a jump to the subharmonic attractor when it is below it. In Figure 8 are shown the coexisting attractors of the primary and subharmonic response at $\Omega = 1{\cdot}758$ and $\alpha_m = 0{\cdot}046$. The curve E_1 in Figure 6 represents the locus of unbounded solutions. For values of Ω to the left of the black dot on E_1, a bifurcation sequence to chaos such as the one shown in Figure 9 is observed. For crossings of E_1 between the black dot and the point of intersection

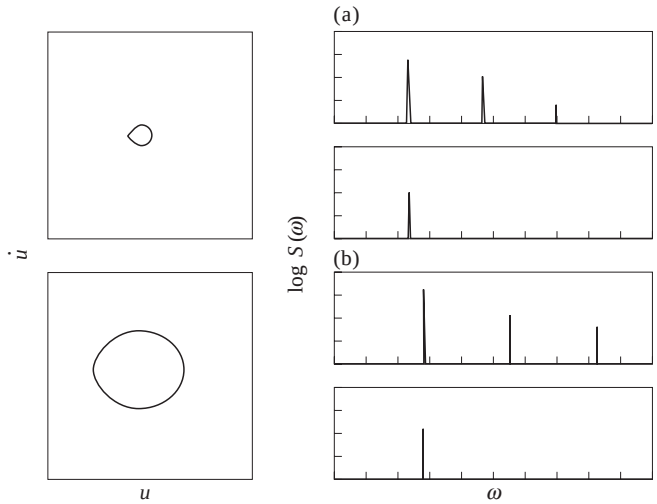

Figure 12. Phase portraits of the attractors near the primary resonance and the power spectra of the response and excitation: (a) $\Omega = 0{\cdot}702$ and $\alpha_m = 0{\cdot}063$; (b) $\Omega = 0{\cdot}827$ and $\alpha_m = 0{\cdot}057$.

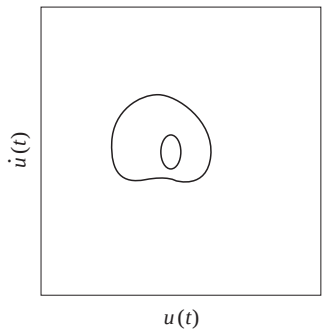

Figure 13. The coexisting attractors near the subharmonic resonance for $\Omega = 1{\cdot}698$ and $\alpha_m = 0{\cdot}061$.

with P_1, a saddle node is observed, making the period-2T solution unstable, and an unbounded solution occurs.

The stability region of the subharmonic is also shown in Figure 6: it is narrower than that in Figure 2. Crossing P_3 from right to left causes the primary resonance to lose stability and the subharmonic becomes stable. Across P_2, the system undergoes period-doubling bifurcations leading to a chaotic attractor, which becomes unstable when E_2 is reached, leading to an unbounded solution. In Figure 10 are shown selected phase planes and power spectra of the above changes in the solution: (a) shows the primary resonance, (b) and (c) show the subharmonic response after crossing P_3, (d) shows a period doubling in the subharmonic after crossing P_2, and (e) shows a second period doubling in the subharmonic response.

In Figure 11 is shown the bifurcation diagram obtained from an analog computer simulation of equation (3) when the bias angle θ_s is set at -6°, and all other parameters are unchanged. In Figure 12 are shown the attractors and power spectra of the primary resonance. Across curve S in Figure 11, the small attractor undergoes a saddle-node bifurcation that leads to an unbounded solution. Across P_1 the large attractor undergoes period-doubling bifurcations. In the portion of P_1 enclosed by E_1, a sequence of period doubling to chaos is observed; in the rest of the curve unbounded solutions occur after the first period doubling. The large attractor also undergoes period-doubling bifurcations across P_4. The subharmonic response undergoes period-doubling bifurcations across P_2, P_3, and P_5. Unbounded solutions are observed after crossing P_2 and E_2. The coexisting attractors that are found between P_2 and P_4 are shown in Figure 13.

6. CONCLUSIONS

From the previous results, we observe that the dynamics of the system significantly depends on the bias parameter, which confirms the experimental observations of Wright and Marshfield [5]. However, it is not possible to conclude which case is more stable, since that depends on the local region of the parameter space under consideration. Nevertheless, the diagrams generated illustrate the overall behavior and the regions of the parameter space where instabilities appear. In Figure 2 are shown the essential features of the primary and subharmonic responses that we analyzed in previous work [3, 4]. However, a very interesting effect appears, which seems to result from the interaction between the parametric and external responses, causing the primary attractor to lose stability around $\Omega = 2$. This behavior is shown in Figures 2, 6 and 11, in spite of the differences in their bifurcation diagrams.

The implications for the physical system are clear. A non-linear system of the type considered, undergoing even very low amplitude oscillations, can suddenly develop large amplitude responses if small excitation changes move the system through a bifurcation.

REFERENCES

1. V. V. Bolotin, 1964 *The Dynamic Stability of Elastic Systems*. San Francisco: Holden-Day.
2. G. Feat and D. Jones, 1981 *International Shipbuilding Progress* **28**, 263–268. Parametric excitation and the stability of a ship subjected to a steady heeling moment.
3. A. H. Nayfeh and N. E. Sanchez 1989 *International Journal of Non llinear Mechanics* **24**(6), 483–497. Bifurcations in a forced softening Duffing oscillator.
4. N. E. Sanchez and A. H. Nayfeh 1990 *International Journal of Non-linear Mechanics* **25**(2), 163–176. Prediction of bifurcations in a parametrically excited Duffing oscillator.
5. J. H. G. Wright and W. B. Marshfield 1980 *Transactions of the Royal Institution of Naval Architects* **122**, 129–148. Ship roll response and capsize behavior in beam seas.
6. C. Y. Liaw and S. R. Bishop 1995 *Nonlinear Dynamics* **8**, 197–211. Nonlinear heave–roll coupling and ship rolling.
7. N. Perez and C. Sanguinetti 1995 *International Shipbuilding Progress* **42**(no. 431), 221–234. Experimental results of parametric resonance phenomenon of roll motion in longitudinal waves for small fishing vessels.
8. J. M. T. Thompson 1989 *Applied Mechanical Reviews* **42**, 15–25. Chaotic dynamics and the Newtonian legacy.
9. C. Kuo and Y. Welaya 1981 *Ocean Engineering* **8**, 65–84. A review of intact stability research and criteria.
10. W. Blocki 1980 *International Shipbuilding Progress* **27**, 36–53. Ship safety in connection with parametric resonance of roll.
11. N. E. Sanchez and A. H. Nayfeh 1990 *International Shipbuilding Progress* **37** (no. 441), 247–272. Nonlinear rolling motions of ships in longitudinal waves.
12. E. C. Zeeman 1977 *Catastrophe Theory*. Reading, Massachusetts: Addison-Wesley.
13. F. Verhulst 1989 *Nonlinear Differential Equations and Dynamical System*. Berlin: Springer-Verlag.
14. A. H. Nayfeh and D. T. Mook 1979 *Nonlinear Oscillations*. New York: Wiley-Interscience.
15. S. Wiggins 1990 *Introduction to Applied Nonlinear Dynamics and Chaos*. Berlin: Springer-Verlag.